

# APPLICATIONS OF METAMATERIALS FOR PARTICLE BEAM DIAGNOSTICS

T. Vaughan\*, V. Antonov, P. Karataev.

John Adams Institute, Royal Holloway University of London, Egham, TW20 0EX, UK

V. Soboleva, RASA Centre in Tomsk, Tomsk Polytechnic University, 632050 Tomsk, Russia

A. Aryshev, High Energy Accelerator Research Organisation (KEK), Tsukuba, Japan

## Abstract

We investigate the application of metamaterials as a tool for particle accelerator beam diagnostics. The optimisation of a metamaterial target with a resonance around 1 THz is presented, along with the proposed experimental layout. A negative refractive index ranging between -1 and -4.6 was achieved over a wide frequency range of 300 GHz.

## INTRODUCTION

Due to their extreme tunability and interesting electromagnetic properties that cannot be found in nature, metamaterials have undergone intense investigation since the late 1990's [1]. In recent years, their applications in accelerator physics have started to be explored. Current areas of interest include; parasitic mode reduction in Radio Frequency (RF) cavities [2], structures for novel acceleration [3] and metamaterial loaded waveguides [4]. For beam diagnostic applications, metamaterials offer advantages over current techniques, such as the electro-optical [5] and RF deflecting cavities [6] because of their extreme flexibility and the fact that a metamaterial target can be used in a non-invasive manner. Furthermore, the material can be tuned to have a negative refractive response over a large frequency range, which is an essential feature for the measurement of a wide spectrum of electron bunch profiles. The negative refractive index also provides a method of improving the signal to noise ratio of the signal, as the signal will be in the reverse direction to most machine backgrounds.

As well as being applicable as a diagnostics tool, the metamaterial target also gives an unprecedented flexibility in terms of the manipulation and transport of radiation. For example, the target could be used to extract a small proportion of the beam's power, say in the terahertz region, to act as a source of terahertz radiation. This is extremely desirable for interdisciplinary research in medicine, biology and chemistry [7, 8].

Considering a single relativistic electron bunch, the total angular power distribution, ignoring any transverse form factors, is given by,

$$\frac{d^2W}{d\omega d\Omega} = \frac{d^2W_e}{d\omega d\Omega} (N_e + N_e(N_e - 1)) |F_z|^2, \quad (1)$$

where  $|F_z|^2$  is the longitudinal form factor, which in turn is the Fourier transform of the longitudinal distribution of  $N_e$  electrons, and  $\frac{d^2W_e}{d\omega d\Omega}$  is the total angular power distribution of

a single electron. When the wavelength under consideration is much larger than the electron bunch length  $\sigma_z$ , the radiation can be considered coherent and the radiation power will be proportional to  $N_e^2$ , instead of just  $N_e$  for the incoherent part of the spectrum. For electron bunch lengths of around 500 fs, which is typical for the first phase of operation at the CLARA FEL test facility [9], radiation of wavelength 1 THz will be in the coherent part of the total angular power spectrum. Additionally, if the electron bunch velocity is faster than the speed of light in the target, the bunch's Coulomb field will generate Cherenkov radiation at the well-defined angle,  $\theta_c$ , given by,

$$\cos(\theta_c) = \frac{1}{\beta n}, \quad (2)$$

where  $n$  is the refractive index of the material and  $\beta$  is the relativistic beam beta.

The aim is to optimise the metamaterial target so that it has a negative refractive index around the 1 THz region. Additionally, because detector sensitivity is not as high around 1 THz as it is at say 0.5 THz, the transmission through the target was also considered during the optimisation process.

## UNIT CELL DESIGN

The unit cell layout is based on the design that was first realised by Smith et al. in 2004 [10]. It consists of two metallic Split Ring Resonators (SRRs) and a metallic bar, separated by a dielectric layer. The SRRs and bar are constructed from Silver as this gives the best trade-off between a high thermal conductivity, which helps avoid local heating due to absorption, and high electrical conductivity, which is essential for a strong resonance. The separating dielectric was chosen to be polyimide.

The layout of the unit cell design can be seen in Fig. 1. Both the SRRs and the bar have a width,  $w_r$  and  $w_b$ , respectively, of 2  $\mu\text{m}$ . The outer and inner SRRs have lengths of  $A = 22 \mu\text{m}$  and  $B = 14 \mu\text{m}$ , respectively, and both have a gap of  $w_g = 6 \mu\text{m}$ . Both the SRRs and bar are patterned as 200 nm thick Silver on top of 20  $\mu\text{m}$  polyimide. The dimension of the substrate layer,  $w_s = 24 \mu\text{m}$  and the spacing between bulk layers was 2  $\mu\text{m}$ .

## SIMULTAION SETUP

All the optimisation procedures were carried out using CST Microwave Studio (CST-MS). This package uses the Finite Integration Technique (FIT) to propagate electromagnetic waves through a structure and extract the scattering,

\* Tom.vaughan.2011@live.rhul.ac.uk

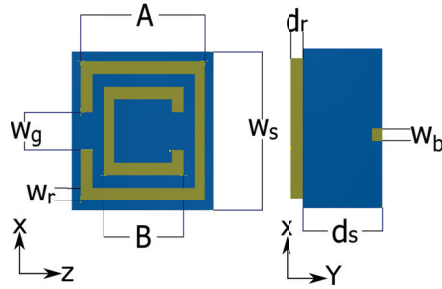


Figure 1: The metamaterial unit cell.

S-parameters. These S-parameters are then converted into the material parameters, i.e. permittivity, permeability, and refractive index, using the method outlined in [11]. Electric and magnetic boundary conditions are used to ensure that the electric and magnetic fields are parallel, polarised in the  $z$  direction, and perpendicular, polarised in the  $y$  direction, to the face of the SSRs, respectively. A plane wave port, combined with an open boundary condition, is used to launch the excitation wave in the positive  $x$  direction. Finally, the frequency range was scanned between 0.8 THz and 1.6 THz.

Clearly there should be no dependence of the S-parameters on the simulation setting such as the Cells per Minimum Wavelength (CMW). Typically, CST recommend this value of CST to be around 10 CMW. However, we found that a value around 20 CMW was needed to ensure that there was no effect on the S-parameter results.

## OPTIMISATION RESULTS

Five of the unit cell parameters,  $d_r$ ,  $d_s$ ,  $w_r$ ,  $w_g$ , and the bulk layer spacing were optimised. For the propose of this paper, the resulting graphs are only shown for the parameters  $d_r$  and  $w_s$ , and for the final optimised unit cell design. The other three parameters were fixed due to the photolithography constraint that the minimum separation between two features must be  $2\ \mu\text{m}$ . The optimisation was carried out using the parameter sweep function in CST-MS. To ensure that the optimisation was consistent and comprehensive, once one parameter had been optimised, the pervious parameters were "re-swept" to account for any additional changes. The results of the optimisation of two of the parameters, the deposition thickness of the rings,  $d_r$ , and substrate dimension of the material,  $w_s$ , are shown in Figs. 3a and 3b, respectively. The blue points represent the value of frequency at which the minimum refractive index occurs. The grey area represents the range of frequency over which the refractive index is negative. The red points show the values of the minimum refractive index.

### Deposition Depth

Figure 3a shows an increase and levelling off of the frequency position of the refractive index minimum. This can be explained using the equivalent circuit for the SRR. The derivation for the capacitance, inductance and resistance as

a function of the dimensions of the unit has been derived in [12]. The resonance frequency,  $f_r$ , of the circuit is given by  $\frac{1}{\sqrt{L \cdot C}}$ , where  $C$  is the total capacitance, taking into account the gap between rings and the gap in each ring, and  $L$  is the total inductance. Although the capacitance and inductance are proportional to the surface area and the volume, respectively, the increase in those value as the deposition depth increases is so small that it can be neglected. The general decrease in the refractive index is caused by the increase in conductive material when the deposition depth is increased. As well as a general decrease, there is also a saw tooth effect consisting of jumps of approximately 4%, which occurs at  $0.752\ \mu\text{m}$  and at  $1.504\ \mu\text{m}$ . These jumps are not yet fully understood and will be examined when the material is manufactured and tested with a terahertz laser [14]. Although both of these trends are positive in the effort to give the metamaterial a negative refractive index in terahertz range, the practicality, cost and experimental ability of depositing a large amount of material needs to be considered. The gain in the minimum of refractive index and the frequency range of negative refraction for larger deposition is not greatly significant for the applications that are being considered. Therefore, the deposition depth was chosen to be  $0.4\ \mu\text{m}$ , as this delivers the best trade-off between the aforementioned parameters.

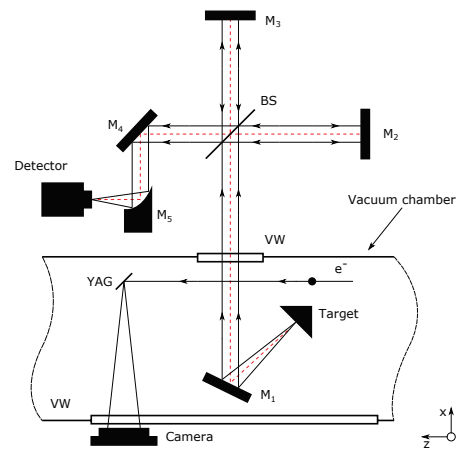


Figure 2: The proposed experimental layout [13].

### Transverse Resonator Spacing

The transverse resonator spacing optimisation was carried out by varying the dimensions of the substrate between 23 and 40 microns, while holding the SRR dimensions constant. It is clear from Fig. 3b that the frequency position reaches a saturation when the substrate width becomes greater than  $32\ \mu\text{m}$ . This saturation can be explained by the fact that the resonance frequency is a function of  $L$  and  $C$ . As the SRR dimensions are constant, once the amount of substrate either side of the SRR is large enough that the homogeneity condition is no longer satisfied, further increases in the substrate dimension will not affect the resonance frequency any further. Figure 3b also shows a minimum and then an increase

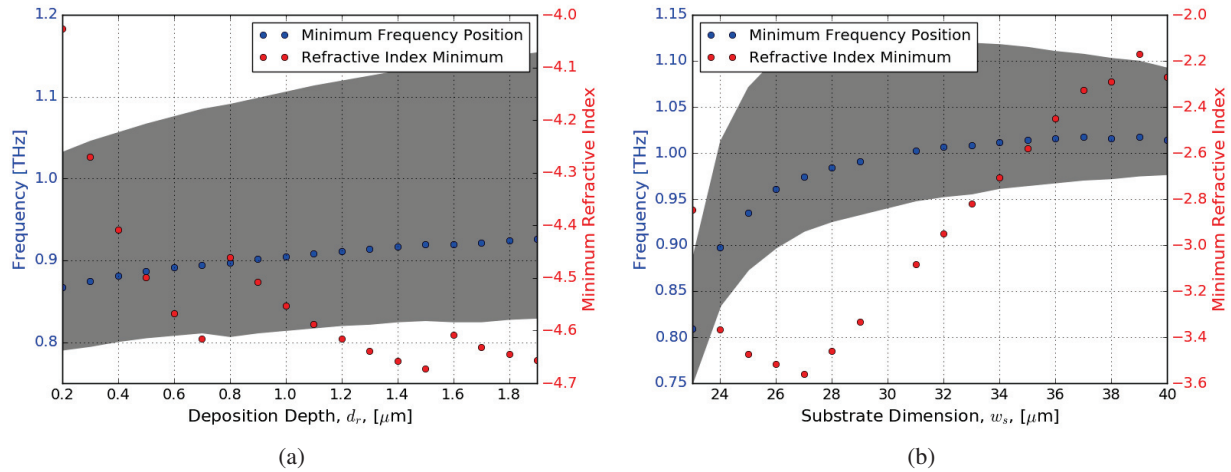


Figure 3: The optimisation results for a) the deposition thickness of the rings, and b) the characteristic dimension of the material. The blue points represent the value of frequency at which the minimum refractive index occurs. The grey area represents the range of frequency over which the refractive index is negative. The red points show the values of the minimum refractive index.

in the minimum of the refractive index for an increasing substrate dimension. This increase is caused by the reduction in the filling factor of the unit cell. The filling factor is the percentage of the unit cell filled by the SRR. As this filling factor is reduced, the effect of the resonator is also reduced. As the negative refractive index is an effect of the resonator, its intensity also decreases.

### Final Resonator Design

Figure 4 shows the frequency dependence of the refractive index and the S-parameters for the optimised unit cell design. S21 represents the fraction of the wave that is transmitted through the sample, while S11 is the fraction of the wave that was reflected. For the purpose of detecting the secondary radiation that is generated during the beam target interaction, the transmission, S21 parameter, should be as large as possible. It is clear from Fig. 4 that for frequencies less than 1 THz, S21 is less than 20% of the incident wave, making detection of those frequencies difficult. However, for frequencies greater than 1.05 THz, at least 50% of the incoming radiation is transmitted. Furthermore, for Cherenkov radiation to be generated, the refractive index can not be in the range  $-1 < n < 1$ . Therefore, the frequency range 1.05 THz to 1.3 THz is the best region for detecting secondary radiation generated by the target.

## EXPERIMENTAL LAYOUT

The experimental layout is shown in Fig. 2. The target is placed at some distance,  $h$ , known as the impact parameter from the electron beam. The target is controlled by a 4D motor, allowing full manipulation of the target’s position. The Cherenkov radiation generated by the target is then directed outside of the vacuum vessel, and into an interferometer, using mirror M1. M1 is fully rotatable allowing the angular

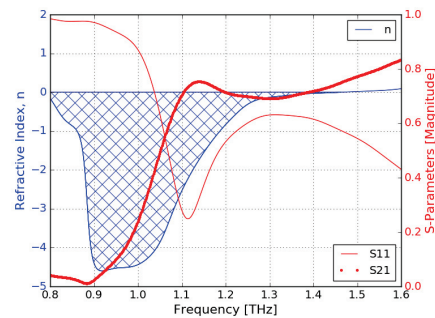


Figure 4: The refractive index, reflection and transmission coefficient as a function of frequency. The cross hatched area shows the region over which the refractive index is negative.

radiation spectrum, as well as the frequency spectrum, to be analysed.

## CONCLUSION

An optimisation process for a metamaterial unit cell has been outlined and applied to develop a metamaterial that possesses a negative refractive index around 1 THz. Further work needs to be completed to convert this unit cell design into a bulk material target that can be used for electron beam diagnostics and terahertz radiation generation. Electron beam simulations will be conducted using CST Particle in Cell solver to test the interaction between the target and electron beam to determine both the best shape for the bulk material and the effect of any beam parameter on the secondary radiation. Once this shape is determined, the bulk material will be manufactured. This bulk material will be tested using a Toptica terahertz laser [14] to verify the simulation results outlined in this paper.

## REFERENCES

- [1] Y. Liu and X. Zhang, “Metamaterials: A New Frontier of Science and Technology”, *Chem. Soc. Rev.*, vol. 40, pp. 2492–2507, 2011.
- [2] A. Danisi, A. Masi and R. Losito “Numerical analysis of metamaterial insertions for mode damping in parasitic particle accelerator cavities”, in *9th Int. Cong. on Advanced Electromagnetic Materials in Microwaves and Optics (META-MATERIALS)*, Oxford, England, 2015, pp. 46–48.
- [3] Y. S. Tan and R. Seviour, “Metamaterial Mediated Inverse Cherenkov Acceleration”, in *Proc. 1st Int. Particle Accelerator Conf. (IPAC’10)*, Kyoto, Japan, May 2010, paper THPD043, pp. 4378–4380.
- [4] F. Meng, Q. Wu, D. Erni and L. Li, “Controllable Metamaterial-Loaded Waveguides Supporting Backward and Forward Waves”, *IEEE Transactions on Antennas and Propagation*, vol. 59, no. 9, pp. 3400–3411, 2011.
- [5] B. Steffen, V. Schlott and F. Muller, “A Compact Single Shot Electro-optical Bunch Length Monitor for the SwissFEL”, in *Proc. 9th European Workshop on Beam Diagnostics and Instrumentation for Particle Accelerators (DIPAC09)*, Basel, Switzerland, 2009, paper TUPB42, pp. 263–265.
- [6] C. Behrens *et al.*, “Few-femtosecond time-resolved measurements of X-ray free-electron lasers”, *Nature Communications*, vol. 5, 2014.
- [7] T. Kampfrath, K. Tanaka and K. A. Nelson, “Light and Non-resonant Control Over Matter and Light .by Intense Terahertz Transients”, *Nature Photonics*, vol. 7, pp. 680–690, 2013.
- [8] D. M. Mittleman, “Frontiers in Terahertz Sources and Plasmonics”, *Nature Photonics*, vol. 7, pp. 666–669, 2013.
- [9] J. Clarke, “CLARA Conceptual Design Report”, *Journal of Instrumentation*, vol. 9, no. 5, 2014.
- [10] D. R. Smith, W. J. Padilla, D. C. Vier, S. C. Nemat-Nasser and S. Schultz “Composite Medium with Simultaneously Negative Permeability and Permittivity”, *Phys. Rev. Letts.*, vol. 84, no. 18, pp. 4184–4187, 2000.
- [11] X. Chen *et al.*, “Robust Method to Retrieve the Constitutive Effective Parameters of Metamaterials”, *Phys. Rev. E*, vol. 70, 2004.
- [12] B. Filiberto *et al.*, “Equivalent-circuit models for the design of metamaterials based on artificial magnetic inclusions”, *IEEE Transactions on Antennas and Propagation*, vol. 55, no. 12, pp. 2865–2873, 2007.
- [13] V. Bleko *et al.*, “Coherent Cherenkov radiation as an intense THz source”, *Journal of Physics: Conference Series*, vol. 732, 2015.
- [14] A. J. Deninger *et al.*, “Precisely Tunable Continuous-wave Terahertz Source with Interferometric Frequency Control”, *Rev. of Scientific Instr.*, vol. 79, no. 4, 2008.